arXiv:2205.09387v1 [cond-mat.mtrl-sci] 19 May 2022

Electronic and Optical properties of TM-doped (8,0) SiC SWNT and the prospect of hydrogen storage

A.T. Mulatu[a,b], K.N. Nigussa[a,*], L.D. Deja[a]

[a]*Department of Physics, Addis Ababa University, P. O. box 1176, Addis Ababa, Ethiopia*
[b]*Department of Physics, Mekelle University, Mekelle, Ethiopia*

Abstract

Properties of transition metal (TM) doped single wall (8,0) SiC nanotube is investigated using first principles density functional theory as implemented within quantum espresso code. The properties studied are electronic, optical, and hydrogen storage prospect, while the transition metals used in the doping are Iron, Manganese, and Cobalt. The outcomes show that ferromagnetic ordering better describes the magnetic order within the doping process. The dopings result in half-metallic property. Hybridization between TM-3d and C-2p near Fermi-level region contributes to occurrence of the half-metallicity property. In addition, optoelectronics character and hydrogen storage capacity of the tube have appeared to be changed compared to that of the pristine. Dopings have appeared to result in an expanded range of optoelectronics applications ranging from photovoltaic effects of far infrared to visible lights. Furthermore, the tube appears to show a potential for hydrogen energy storage.

Keywords: Zizag Nanotube, DMS, Hydrogen, DFT, Optoelectronics, Half-metallic.

1. Introduction

A scientific pursuit for investigating efficient materials for optoelectronic analysis [1, 2] and hydrogen storage applications is continuing unabated [3, 4]. Extracting energies using photovoltaic effect and from hydrogen energy is recently getting increased attention since it adheres to global priority area of searching for renewable energies. A range of applications such as spintronics are exhibited from half-metallicity properties [5, 6]. Literature review [3] show that studies on Alkali-metal doped SiC nanotube revealed some prospect of hydrogen energy storage. Doping of Fe is studied with various systems such as ZnO [7], and doping of Mn has been studied with GaP [6]. However, up to date, the authors do not find sufficient literature document on doping of SiC nanotube with Fe, Mn, and Co, and the respective impacts on the electronic, optical, and hydrogen storage properties. Zigzag SiC SWNT show a direct bandgap in a semiconductor region [8] while other chiralities such as armchair SWNT may, however, show indirect bandgaps [2]. Thus, we believe that doping zigzag SiC SWNT may be better suitable for bandgap tuning for applications in half-metallicity and optoelectronics.

Silicon bulk system has been known for its good applications in photovoltaics [9] due its bandgap of around 1.1 eV [10]. Meanwhile, carbon-graphite is known for its electrical conductor nature with narrow or no bandgap [11]. Silicon carbide bulk is expected to have bandgap of 2.2 eV [10]. In our previous work [8], we have reported that nanotubes have bandgaps smaller than the bulk counterpart but where the bandgaps approach closely to that of the bulk value for zigzag chiralities greater or equal to (6,0). By doping, the bandgaps would be likely to be reduced from the value corresponding to the pristine, and thus would imply different electrical as well as optoelectronics application properties.

*Corresponding author: kenate.nemera@aau.edu.et (K.N. Nigussa)
Email addresses: abebetadesse2@gmail.com (A.T. Mulatu), lemi.demeyu@aau.edu.et (L.D. Deja)

Dilute magnetic semiconductor (DMS) property is reported to be exhibited by doping semiconductors with transition metals [12, 13]. DMSs often exhibit half-metallic property and can undergo a transition from ferromagnetic state to paramagnetic state at a temperature called critical temperature, which is calculated by

$$T_c = \frac{2\Delta E_{FM}}{3k_B n} \tag{1}$$

as described in literature [12], where k_B is the Boltzmann constant, n is the number of doping atoms, and ΔE_{FM} is the difference between total energies in the ferromagnetic and antiferromagnetic ordering. The prospect of occurrence of such property in (8,0) SiC SWNT is studied by doping with Fe, Mn, & Co. Dopant concentration x is described as the fraction ratio of number of dopant atoms to number of Silicon atoms in the unit cell of the pristine. Thus, $x = 0.0625$, and $x = 0.125$ are considered in this study. With consideration of the dopant atoms Fe, Mn, and Co, we expect to investigate the relative prospects of applications in spin injection as well as at which concentartions do such applications become optimal. The paper is organized as follows. In the next section (sec. 2), a detail account of the computational method is presented. Results and discussion are presented in section 3, with the conclusion being presented in section 4.

2. Computational Methods

An ab-initio simulations within quantum espresso code [14] is used to examine the electronic structure and optical properties of the zigzag (8,0) SiC SWNT. The electron wavefunction is expanded over a plane wave basis set. The electron-ion interactions is approximated within projector augmented wave (PAW) modality (PAW data set) [15] upon the calculation of electronic properties and geometry optimizations. Upon optical properties calculations, the electron-ion interactions is approximated within norm conserving pseudopotential [16]. The exchange-correlation energies are treated using PBE [17]. The k-points of the Brillouin zone (BZ) are generated from the input **k**-mesh using the Monkhorst-Pack scheme [18]. The number of valence electrons considered for each element within the paw data sets is Fe:8, Mn:7, Co:9, H:1, C:4, and Si:4. Geometry relaxations are carried out using BFGS minimizer [19], where optimizations of the atomic coordinates and the unit cell degrees of freedom is done within the concept of the Hellmann-Feynman forces and stresses [20, 21] as calculated on the Born-Oppenheimer (BO) surface [22]. The convergence criteria for the forces were set at 0.05 eV/Å.

The optimum magnetic moments of 4.0 μ_B, 3.0 μ_B, and 3.0 μ_B, is placed on each Fe, Mn, & Co atoms, respectively. Dopings is done by replacing two or four silicon atoms with the dopant transition metal atoms. The favored magnetic ordering is ferromagnetic. When the number of dopant atoms is two, the total magnetic moment per unit cell 8.0 μ_B, 6.0 μ_B, 6.0 μ_B, respectively, for Fe, Mn, and Co. When the number of dopant atoms is four, the total magnetic moment per unit cell 16.0 μ_B, 12.0 μ_B, 12.0 μ_B, respectively, for Fe, Mn, and Co. The pristine nanotube unit cell contains 64 atoms with Si:C ratio being 1:1, and has a tetragonal lattice vectors $a = b = 15.9$ Å and $c = 10.8$ Å, with periodic boundary conditions being allowed along the c-lattice vector, and a zero chirality angle. Along the a & b lattice vectors, a vacuum space of 10 Å is placed to make sure that no lateral interaction occurs between adjacent unit cells.

Formation energy (eV/atom) is calculated as

$$E_f = \mu_t - \mu_{Si} - \mu_C - \mu_{dopant} \tag{2}$$

where μ_t is total chemical potential of the system containing dopant and tube, μ_{Si} is chemical potential of bulk Silicon crystal, μ_C is chemical potential of bulk Carbon crystal in graphite structure, & μ_{dopant} is chemical potential of the dopant atom. Iron, Manganese, and Cobalt are dopant atoms considered in this work. Chemical potentials are calculated as total energy divided by the number of atoms in the unit cell of the bulk crystals, while for the nanotube, it is given by total energy divided by number of SiC pairs, & for dopant atoms it is the same as total energy of single free atom. Free atom is modelled by putting single atom in a cubic super unit cell of side length 10 Å.

Adsorptions are done by putting adsorbate molecules on the tube & then allowing geometry relaxations to take

place. Adsorption energy is calculated as

$$E_{ads} = -(E_{(t\ +\ nH_2)} - E_t - E_{nH_2}) \tag{3}$$

where $E_{(t\ +\ nH_2)}$ is total energy of the system containing tube & adsorbate hydrogen, E_t is total energy of clean tube, & nE_{H_2} is total energy of adsorbate hydrogen. E_{H_2} is total energy of a single free hydrogen molecule, which is obtained by optimizing in a cubic supercell of side length 10 Å. The number of adsorbate molecules used in the adsorption is indicated by n. According to Eq. (3), positive values of E_{ads} means exothermic process, while negative values mean endothermic. A van der Waal's treatment within DFT-D3 [23] is applied wherever necessary. The **k**-mesh of 1×1×15 and a cut-off energy (ecut) of 600 eV is used in the calculations.

Hubbard U correction [24] is applied to the dopant atoms. We have selected U=7 eV to be optimum to our system. Spin polarized calculation is allowed. Density of states (DOS) is calculated as a population of states in the spin-up and spin-down states at the chosen energy windows. Projected DOS (PDOS) is calculated as a component of DOS resolved onto atomic orbitals. To characterize optical properties, a dielectric function is computed, which has generally a complex nature & is given as

$$\varepsilon(\omega) = \varepsilon_1(\omega)\ +\ i\,\varepsilon_2(\omega) \tag{4}$$

The imaginary part $\varepsilon_2(\omega)$ is calculated from the density matrix of the electronic structure [25] as described elsewhere [26], & given by

$$\varepsilon_2(\omega) = \frac{8\pi^2 e^2 \hbar^2}{\Omega \omega^2 {m_e}^2} \sum_{k,v,c} w_k |\langle \psi_k^c | \mathbf{u}\cdot\mathbf{r} | \psi_k^v \rangle|^2 \delta(E_k^c - E_k^v - \hbar\omega), \tag{5}$$

where e is the electronic charge, and ψ_k^c and ψ_k^v are the conduction band (CB) and valence band (VB) wave functions at k, respectively, $\hbar\omega$ is the energy of the incident phonon, $\mathbf{u}\cdot\mathbf{r}$ is the momentum operator, w_k is a joint density of states, & Ω is volume of the primitive cell. The real part $\varepsilon_1(\omega)$ can be extracted from the imaginary part of Eq. (5) according to Kramer-Kronig relationship [27], as follows.

$$\varepsilon_1(\omega) = 1\ +\ \frac{2}{\pi} P \int_0^\infty \frac{\omega' \varepsilon_2(\omega')}{\omega'^2 - \omega^2} d\omega' \tag{6}$$

where P is a principal value. The electron energy loss function ($L(\omega)$), as given elsewhere [28], is calculated by

$$\frac{\varepsilon_2(\omega)}{\varepsilon_1^2(\omega) + \varepsilon_2^2(\omega)} \tag{7}$$

The joint density of states (JDOS) is defined as

$$n(\omega) = \sum_\sigma \sum_{n\in V} \sum_{n'\in C} \frac{\Omega}{(2\pi)^3} \int \delta(E_{k,n'} - E_{k,n} - \hbar\omega) d^3\mathbf{k} \tag{8}$$

were σ is the spin component, Ω is the volume of the lattice cell, n and n' belong to the valence and conduction bands, respectively, and $E_{k,n}$ and $E_{k,n'}$ are the corresponding eigenvalues.

3. Results and discussion

As can be seen from table 1, the formation energies have positive and negative values. According to Eq. (2), negative values means exothermic, while positive values means endothermic process. Thus, the dopings somehow result in less stable structures as compared to the pristine. However, increasing concentration of dopant seems to increase back the stabilities of structures but where the latter stabilities are still lower than that of the pristine. The critical temperatures are calculated according to Eq. 1, and show increases in values when the dopant concentration increases.

Table 1: Concentration of dopant (x), Half-metallic energy gap (HM_g) in eV, Formation energy (E_f) in eV/atom, Total energy per atom (E) in eV/atom, Energy gap (E_g) in eV, and critical temperature T_c in Kelvin, for doped and pristine (8,0) SiC SWNT.

System	x	E_g (eV)	E_f (eV/atom)	E (eV)	HM_g (eV)	T_c (K)
Pristine	-	1.10	-1.09	-9.59	-	-
Fe-doped	0.0625	0.80	3.65	-17.05	0.38	-
	0.1250	1.59	1.47	-24.65	0.81	61.89
	0.1875	1.69	1.73	-32.17	0.43	-
	0.2500	2.12	0.56	-39.74	0.29	385.29
Co-doped	0.1250	1.29	-1.22	-26.44	1.14	527.04
	0.1875	1.58	8.48	-34.83	1.20	311.00
	0.2500	1.93	11.20	-43.24	1.36	
Mn-doped	0.0625	1.14	5.92	-15.87	0.52	
	0.1250	0.88	-113.97	-22.45	0.30	108.31
	0.1875	1.54	-163.53	-28.42	1.26	638.11
	0.2500	1.97	7.307	-34.74	1.45	622.33

3.1. Electronic properties of TM doped (8,0) SiC SWNT

By doping Fe, the bandgap seems to increase with increasing concentration of dopant while half-metallic bandgap seems to decrease (see table 1). The values of HM_g are w[illegible]

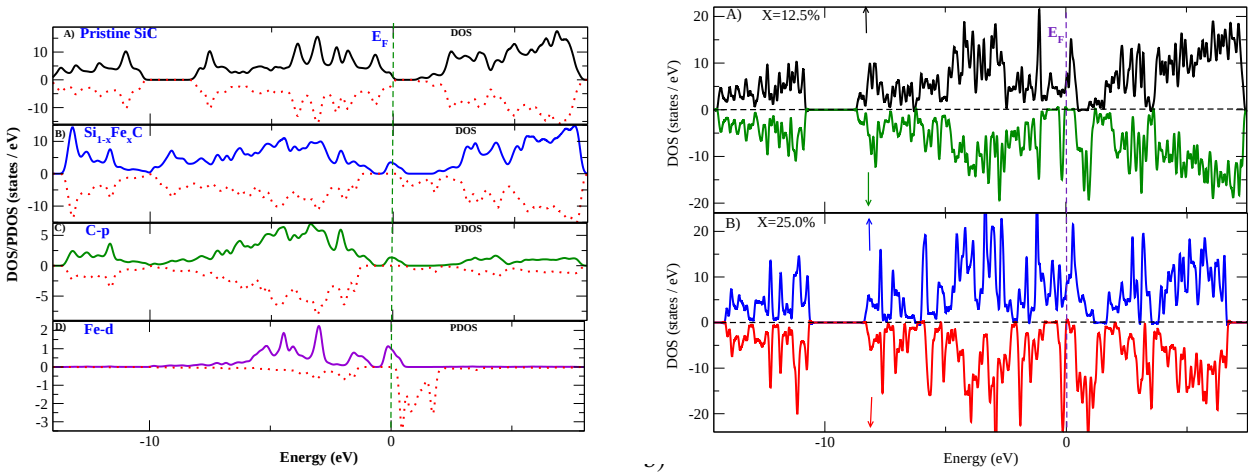


Figure 1: a) Left side. PDOS of $Si_{1-x}Fe_xC$ (x = 0.0625) compound. b) Right side. DOS for majority/minority spin channels (MAC/MIC) is shown by +ve/-ve value. X is meant for percentage form of x.

half-metallicity property since both spin-up and spin-down channels do not cross the Fermi-level. However, by the introduction of the dopant Fe, the DOS of MAC shows crossing of the Fermi-level while the MIC shows a gap (see right side of the figure). Meanwhile, the PDOS (left side of Fig. 1, lower parts) show that the hybridization between Fe-3d and O-2p is resulting to the non-zero DOS values of the majority spin channel.

With Cobalt and Manganese doped SiC SWNT, the bandgap and half-metallic gap seem to increase by increasing dopant concentrations (see table 1). Thus, Co doping seems to show little significance for application in spintronics,

within the range of dopant concentration considered in this study. However, Manganese doping can be applied in spintronics application at lower dopant concentrations of up t

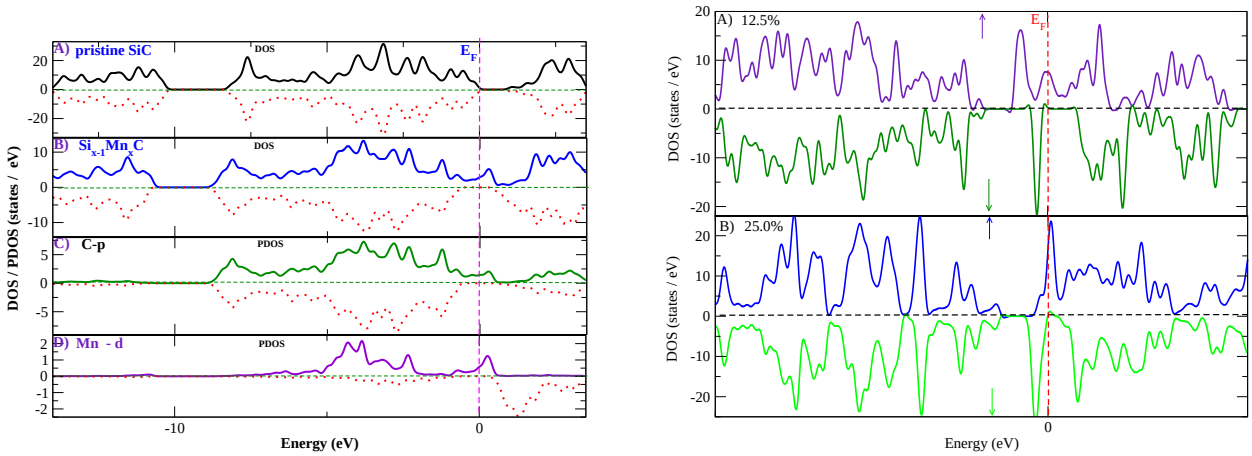


Figure 2: a) Left side. PDOS of $Si_{1-x}Mn_xC$ ($x = 0.0625$) compound. b) Right side. DOS for majority/minority spin channels (MAC/MIC) is shown by +ve/-ve value. X is meant for percentage form of x.

The DOS of pristine on the left side of Fig. 2, top part, shows no half-metallicity property since both spin-up and spin-down channels do not cross the Fermi-level. However, by the introduction of the dopant Mn, the DOS of MAC shows crossing of the Fermi-level while the MIC shows a gap (see right side of the figure). Meanwhile, the PDOS (left side of Fig. 1, lower parts) show that the hybridization between Mn-3d and O-2p is resulting to the non-zero DOS

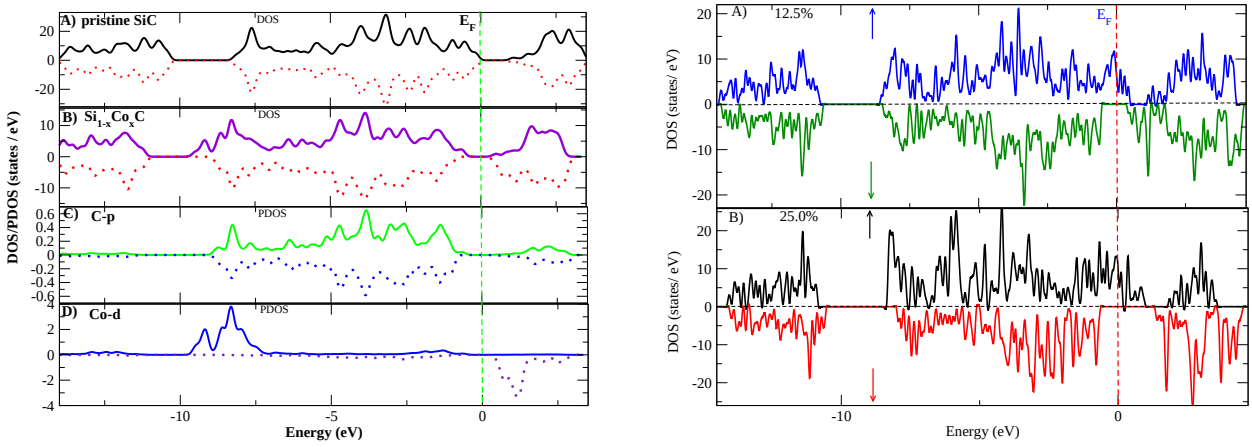


Figure 3: a) Left side. PDOS of $Si_{1-x}Co_xC$ ($x = 0.0625$) compound. b) Right side. DOS for majority/minority spin channels (MAC/MIC) is shown by +ve/-ve value. X is meant for percentage form of x.

property since both spin-up and spin-down channels do not cross the Fermi-level. However, by the introduction of the dopant Co, the DOS of MAC shows crossing of the Fermi-level while the MIC shows a gap (see right side of figure). However, this happens only at higher Co dopant concentration, starting at $x = 0.125$. Meanwhile, the corresponding PDOS show that the hybridization between Co-3d and O-2p is resulting to the non-zero DOS values of the majority spin channel.

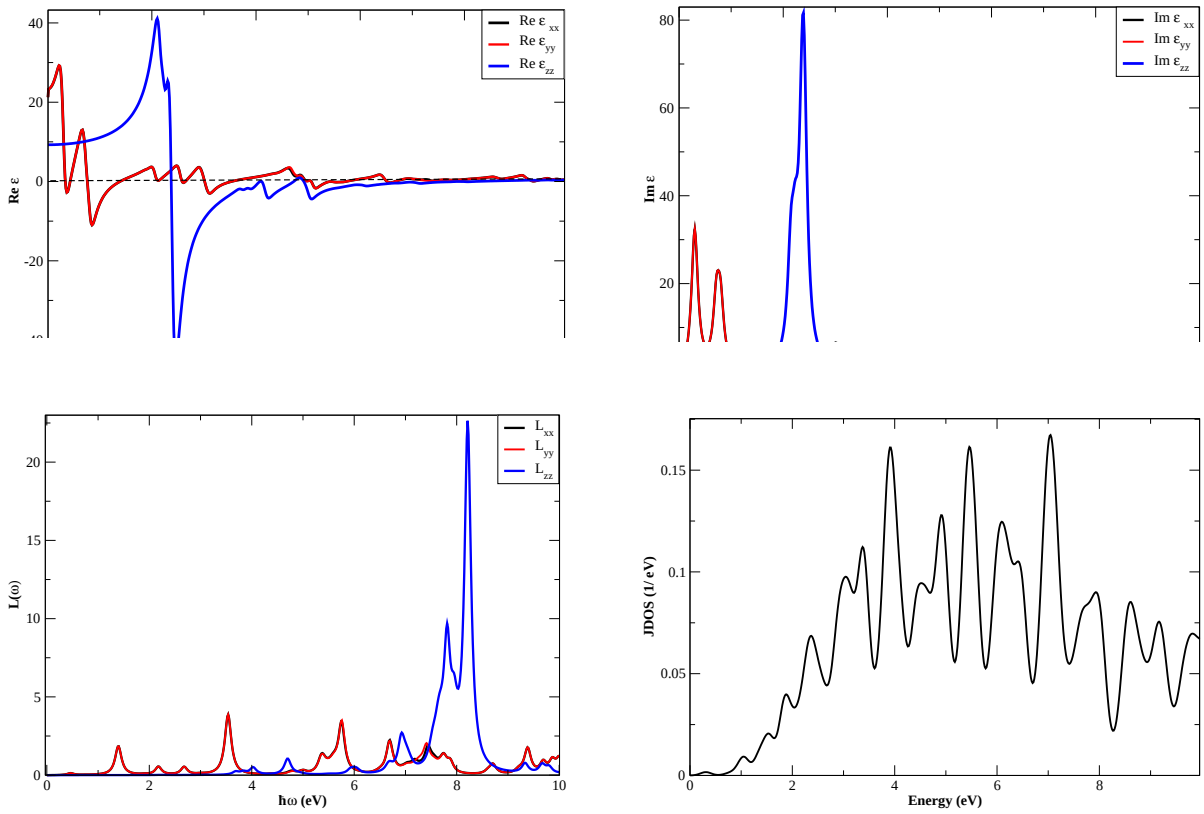


Figure 4: Optical properties of pristine (8,0) SiC SWNT. a) Top left. Real part of the dielectric function calculated according Eq. (6). b) Top right. Imaginary part of dielectric function calculated according to Eq. (5). c) Bottom left. Electron energy loss calculated according to Eq. (7). d) Bottom right. JDOS calculated according to Eq. (8).

3.2. Optical Properties of TM doped (8,0) SiC SWNT

We present optical properties of pristine in Fig. 4 to reveal differences as compared the doped counterparts (Figs. 5 & 6). It looks that the real component of the dielectric function has non-zero value in the photon energy ranges of up to 3.0 eV. $\varepsilon(0)$=20, and ε_1 approaches zero at higher photon energies exceeding 4.0 eV. Conditions of applicability in plasmonic effect may also be significant at photon energies of near 8.0 eV. The optical absorption peak seems to appear near photon energy range of 2.0 eV. This makes it a possible candidate for photovoltaic effect of orange and red light. Direction resolved optical property is presented and it shows that directional interaction of light along the tube z-axis dominates the contribution to the optical property. JDOS shows population of holes created due to excitation of electrons. As shown in figure (bottom right), the JDOS has significant values at the photon energies exceeding 1.0 eV, with peaks occurring in the photon energy ranges of 4.0-7.0 eV.

Optical property with Fe doped (8,0) SiC SWNT is presented in Fig. 5. $\varepsilon(0)$=30 and shows increases compared to the pristine. Non-zero optical absorption happens at photon energies from 0.3-2.5 eV. The absorption property at photon energies of 0.3-1.5 eV occurs due to the Fe doping introduced to the system. At these absorption regime, the application as detectors or sensors, as well as photovoltaic effect of red and near infrared light is likely a favourite. In the absorption regime exceeding 1.5 eV but up to 2.5 eV, a photovoltaic effect of green and blue light may dominate. JDOS possesses non-zero values beginning from photon energies exceeding 0.2 eV, where a widening peaks happen at photon energies between 3.0-7.0 eV. Energy loss function may show application in plasmonic effect near photon energies of 8.0 eV. Optical property of Co doped (8.0) SiC SWNT is presented in Fig. 6. The properties investigated seem to be closely similar to the presentation of the case of Fe doped (8,0) SiC SWNT (Fig. 5). It seems that the cobalt doping could result to significant photovoltaic effects of green and blue light, while also possibly important for applications in sensors and detectors. Energy loss function may show applications in plasmonic effect at photon

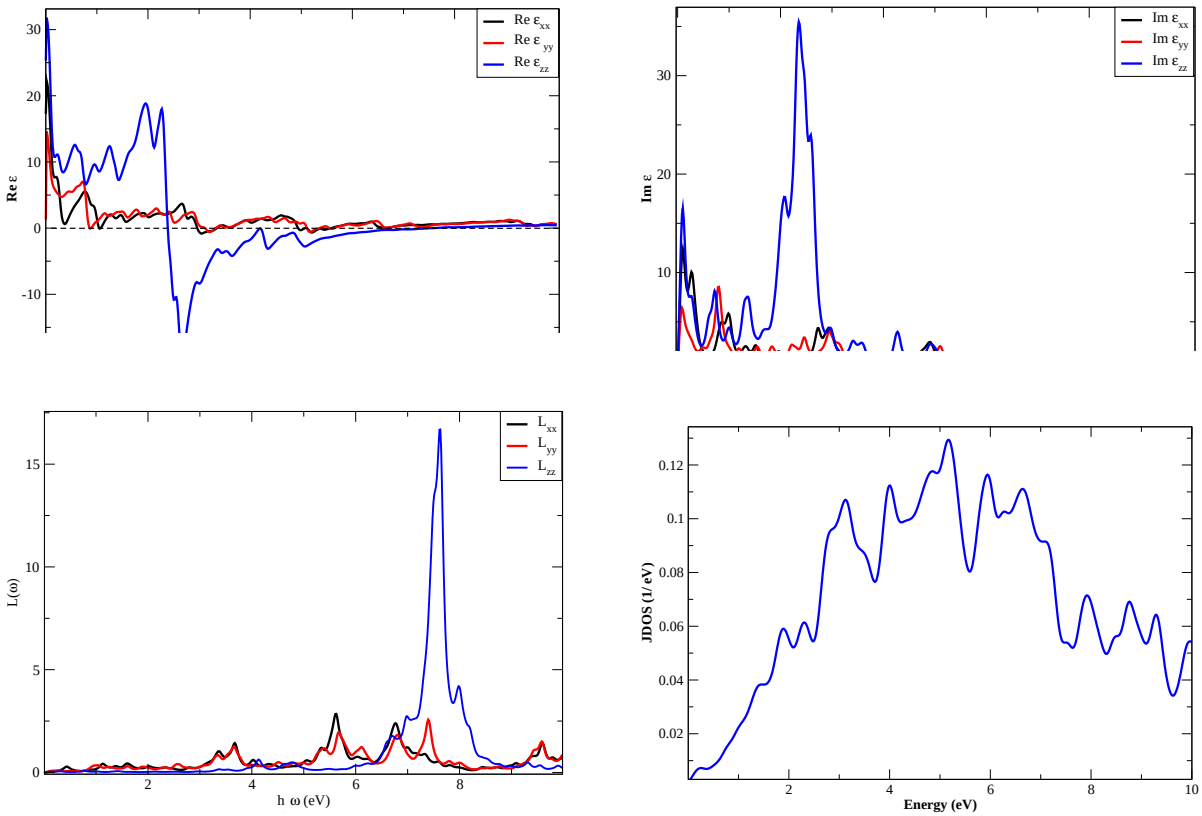


Figure 5: Optical properties of Fe-doped (8,0) SiC SWNT. a) Top left. Real part of the dielectric function calculated according Eq. (6). b) Top right. Imaginary part of dielectric function calculated according to Eq. (5). c) Bottom left. Electron energy loss calculated according to Eq. (7). d) Bottom right. JDOS calculated according to Eq. (8).

energies near 8.0 eV.

3.3. Hydrogen adsorption on pristine and TM doped (8,0) SiC SWNT

Table 2: Formation energy (E_f) in eV, Total energy per atom (E) in eV/atom, Adsorption energy (E_{ads}) in eV, and n is number of hydrogen molecule adsorbed (Eq. (3)) on pristine (8,0) SiC SWNT.

Site	n	E_{ads} (eV)	E_f (eV/atom)	E (eV/atom)
	2	-1.62	1.96	-9.09
	4	1.78	0.76	-8.63
Out	6	3.84	-1.12	-8.23
	8	5.90	-4.11	-7.87
	2	-0.29	0.96	-9.07
In	4	1.67	0.85	-8.62
	6	3.70	-1.03	-8.22
	8	5.61	-3.91	-7.86

From table 2, it looks that adsorption energy increases by increasing the concentration of hydrogen molecule. The increases happen for both the *In* and *Out* sites (Fig. 7). From the adsorption energy and formation energy, we

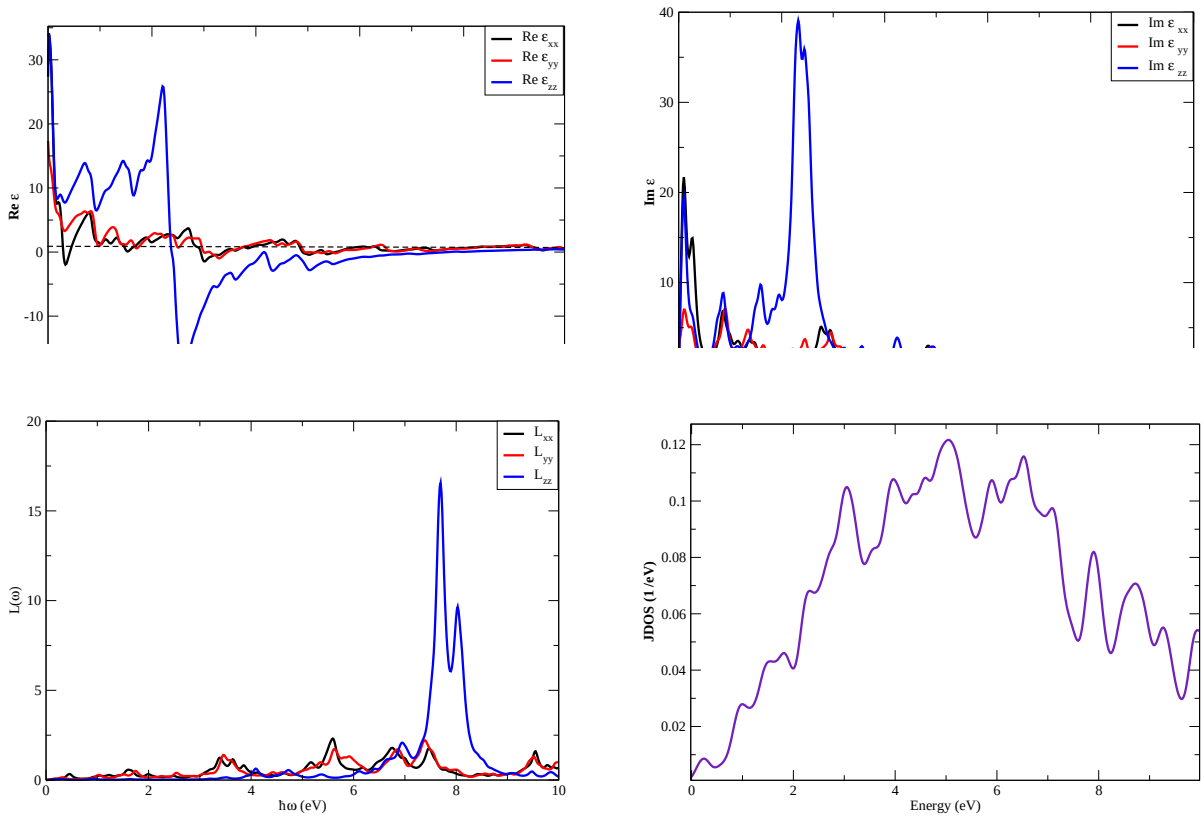


Figure 6: Optical properties of Co-doped (8,0) SiC SWNT. a) Top left. Real part of the dielectric function calculated according Eq. (6). b) Top right. Imaginary part of dielectric function calculated according to Eq. (5). c) Bottom left. Electron energy loss calculated according to Eq. (7). d) Bottom right. JDOS calculated according to Eq. (8).

can see that the formation energy becomes exothermic at higher n molecules adsorbed. The formation energy shows endothermic process for n=2 and n=4, while an exothermic process for n=6 and n=8. This applies to both the *In* and *Out* sites. Thus, the formation energy analysis suggests that stability increases with increased n. The *Out* site has relatively an edge over the *In* site for adsorptions. The adsorption energies seem to be relatively larger for adsorptions at the *Out* site when compared to that of the *In* site. At lower adsorbate amount of below n=2, it seems that the *In* site is more favourable adsorption site compared to that of the *Out* site. However, when the adsorbate amount exceeds n=2, there is a switch in the favorability, where the *Out* site becomes more favourable adsorption site compared to the *In* site. Furthermore, when the amount of adsorbate exceeds n=6, the adsorption process experiences more binding strength to the tube and thus can be described by formation as a compound. This latter phenomena can be relevant to the concept of hydrogen energy storage.

From the Fig. 7 (lower sides), it seems that the adsorption may not change the electric property of the pristine from being a semiconductor. The optical property studied following adsorption of hydrogen is given in Fig. 8. By adsorption of hydrogen, in addition to the optical property along the tube z-axis, the optical property along the tube's y-axis also becomes significant. As a result, applications in photo-sensors and detectors dominate in photon energy ranges of up to 1.1 eV, while application in photovoltaic effect of near infrared and red lights dominate in photon energies range exceeding 1.1 eV but up to 2 eV. Plasmonic effects can potentially take place at lower photon energies such as at photon energies of around 5.0 eV, compared to the counterpart in pristine or TM doping.

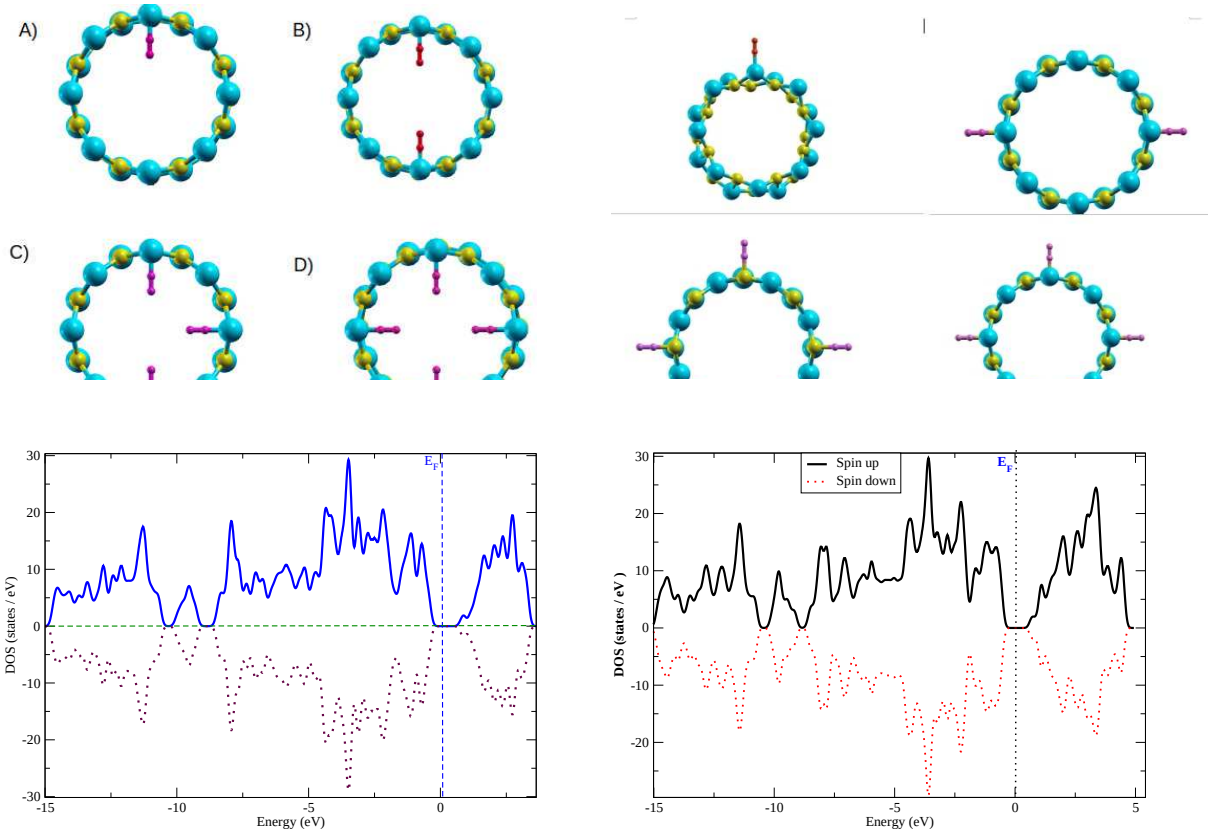


Figure 7: Upper side. The geometries of adsorptions on the inside and outside sites (see table 2). Lower side. Corresponding density of states.

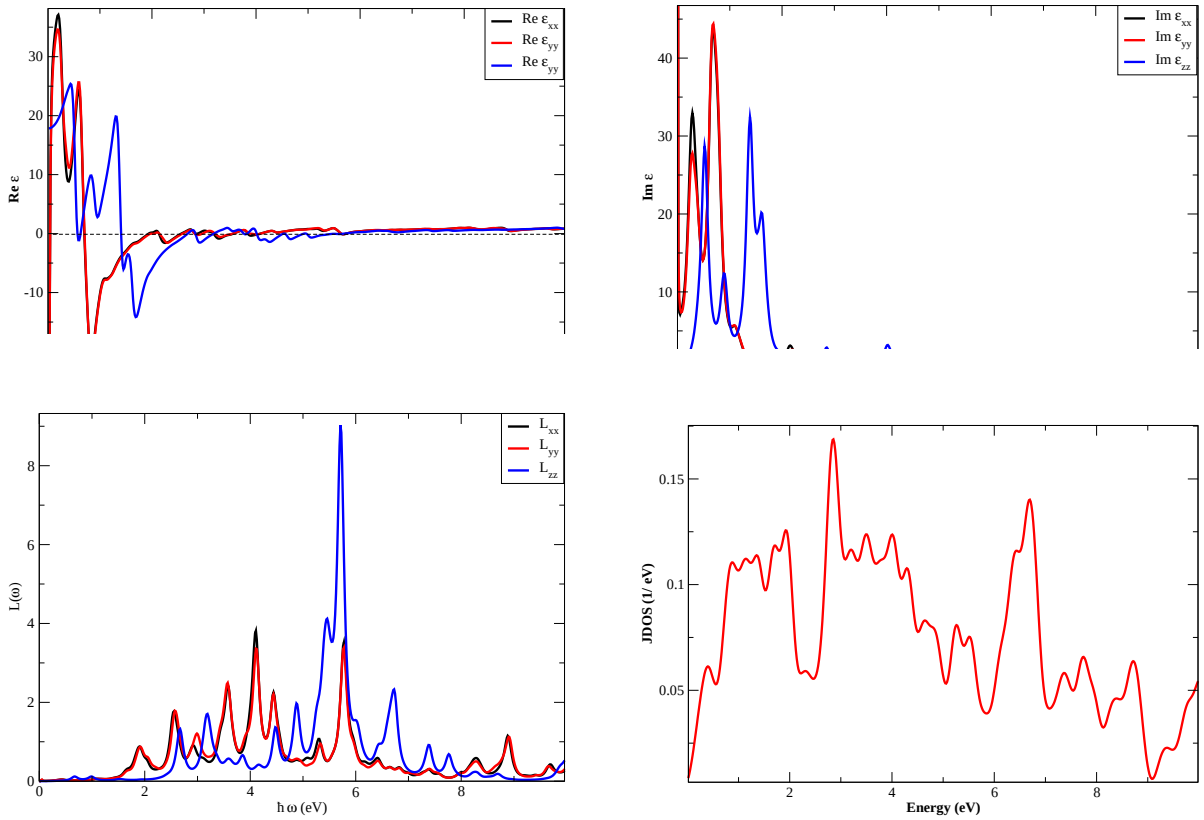


Figure 8: Optical properties of pristine (8,0) SiC SWNT after hydrogen adsorbed. a) Top left. Real part of the dielectric function calculated according Eq. (6). b) Top right. Imaginary part of dielectric function calculated according to Eq. (5). c) Bottom left. Electron energy loss calculated according to Eq. (7). d) Bottom right. JDOS calculated according to Eq. (8).

4. Conclusion

The typical outputs of this study can be summarized as follows.

- Doping with Fe, Co, or Mn appears to expand the range of optoelectronics application of the tube. Potential expanded applications include photovoltaic effects in a broad range of from far infrared light to visible light.
- Doping of Fe and Mn have the potential to lead to half-metallic property with a possible application in spintronics.
- Hydrogen storage seems to have a good promising opportunity on (8,0) SiC SWNT. This pinpoints its potential relevance to the hydrogen energy storage application.
- Adsorption of hydrogen seems to impact on optical property of the tube by widening the scope of application in optoelectronics as similar with the impacts that the dopings offer. This effect can be particularly noticeable when the amount of adsorbed hydrogen (nH_2) is large, i.e., where $n \geq 6$. The adsorbed hydrogen prefers to interact with silicon atoms of the tube than carbon atoms. Furthermore, the adsorbates bind to the tube preferably on the outside of the tube than on the inside of the tube.
- Direction resolved analysis of the interaction of light with the tube indicates that the tube as a pristine or in a doped status dominantly interacts along its periodic z-axis. But in the case of hydrogen being already adsorbed, significant interaction along the tube's non-periodic y-axis happens in addition to the periodic z-axis.
- The tube in its pristine or doped status appears to have significance for plasmonic effect and photonics applications at photon energies in the far ultraviolet light (i.e., ca $\hbar\omega$=8 eV).

Disclosure statement

The authors declare that there is no conflict of interest.

Acknowledgments

We are grateful to the Ministry of Education of Ethiopia for financial support. The authors also acknowledge the International Science Program, Uppsala University, Sweden, for providing computer facilities for research at the Department of Physics. The office of VPRTT of Addis Ababa university is also warmly appreciated for supporting this research under a grant number AR/032/2021.

ORCID iDs

K.N. Nigussa.
https://orcid.org/0000-0002-0065-4325.

References

References

[1] W. Wang, J. Xu, Y. Zhang, G. Li, First-Principles Study of Electronic Structure and Optical Properties of Silicon/Carbon Nanotube, Computational Chemistry, 5 (2017) 159–171.

[2] C. Vatankhah, H. Badehian, Electronic and optical properties of armchair silicon carbide nanotubes from first principles, Optik 237 (2021) 166740.

[3] X. Wang, K. M. Liew, Hydrogen storage in Silicon Carbide Nanotubes by Lithium Doping, The Journal of Physical Chemistry C 115 (8) (2011) 3491–3496.

[4] L. Arellano, F. de Santiago, A. Miranda, F. Salazar, A. Trejo, L. Pérez, M. Cruz-Irisson, Hydrogen storage capacities of alkali and alkaline-earth metal atoms on SiC monolayer: A first-principles study, International Journal of Hydrogen Energy 46 (38) (2021) 20266–20279.

[5] M. Boutaleb, A. Tadjer, B. Doumi, A. Djedid, A. Yakoubi, F. Dahmane, B. Abbar, First-Principle Investigations of Structural, Electronic, and Half-Metallic Ferromagnetic Properties in $In_{1-x}TM_xP$ (TM = Cr, Mn), J Supercond Nov Magn 27 (2014) 1603.

[6] B. Doumi, A. Mokaddem, A. Sayede, M. Boutaleb, A. Tadjer, F. Dahmane, Half-Metallic Ferromagnetic Property Related to Spintronic Applications in 3d (V, Cr, and Mn)-Doped GaP DMSs, J. Supercond Nov Magn 28 (2015) 3163–3172.
[7] G. Shaoqiang, H. Qingyu, X. Zhenchao, Z. Chunwang, First principles study of magneto-optical properties of Fe-doped ZnO, Physica B: Condensed Matter 503 (2016) 93–99.
[8] A. Mulatu, K. Nigussa, L. Deja, Structural and electronic properties of zigzag single wall (8,0), (9,0), and (10,0) silicon carbide nanotubes, Materialia 20 (2021) 101257.
[9] M. Alaaeddin, S. Sapuan, M. Zuhri, E. Zainudin, F. AL- Oqla, Photovoltaic applications: Status and manufacturing prospects, Renewable and Sustainable Energy Reviews 102 (2019) 318–332.
[10] H. Morkoç, S. Strite, G. Gao, M. Lin, B. Sverdlov, M. Burns, Large-band-gap SiC, III-V nitride, and II-VI ZnSe-based semiconductor device technologies, Journal of Applied Physics 76 (1994) 1363.
[11] H. Zhu, J. Wei, K. Wang, D. Wu, Applications of carbon materials in photovoltaic solar cells, Solar Energy Materials and Solar Cells 93 (2009) 1461–1470.
[12] M. Zhang, J. Huang, X. Liu, L. Lin, H. Tao, Electronic Structure and High Magnetic Properties of (Cr, Co)-codoped 4H-SiC Studied by First-Principle Calculations, Crystals 10 (2020) 634.
[13] K. Sato, H. Katayama-Yoshida, P. Dederichs, Curie temperatures of III-V diluted magnetic semiconductors calculated from first principles, Journal of Superconductivity 16 (2003) 31–35.
[14] P. Giannozzi, S. Baroni, N. Bonini, M. Calandra, R. Car, C. Cavazzoni, D. Ceresoli, G. L. Chiarotti, M. Cococcioni, I. Dabo, A. D. Corso, S. de Gironcoli, S. Fabris, G. Fratesi, R. Gebauer, U. Gerstmann, C. Gougoussis, A. Kokalj, M. Lazzeri, L. Martin-Samos, N. Marzari, F. Mauri, R. Mazzarello, S. Paolini, A. Pasquarello, L. Paulatto, C. Sbraccia, S. Scandolo, G. Sclauzero, A. P. Seitsonen, A. Smogunov, P. Umari, R. M. Wentzcovitch, QUANTUM ESPRESSO: a modular and open-source software project for quantum simulations of materials, Journal of Physics: Condensed Matter 21 (2009) 395502.
[15] P. Blöchl, Projector augmented-wave method, Phys. Rev. B 50 (1994) 17953.
[16] L. Kleinman, D. M. Bylander, Efficacious form for model pseudopotentials, Phys. Rev. Lett. 48 (1982) 1425–1428.
[17] J. Perdew, K. Burke, M. Ernzerhof, Generalized Gradient Approximation Made Simple, Phys. Rev. Lett. 77 (1996) 3865.
[18] H. Monkhorst, J. Pack, Special points for Brillouin-zone integrations, Phys. Rev. B 13 (1976) 5188.
[19] H. Schlegel, Optimization of equilibrium geometries and transition structures, J. Comp. Chem. 3 (1982) 214.
[20] P. Feynman, Forces in Molecules, Phys. Rev. 56 (1939) 340.
[21] O. Nielsen, R. Martin, Quantum-mechanical theory of stress and force, Phys. Rev. B. 32 (1985) 3780.
[22] R. Wentzcovitch, J. Martins, First principles molecular dynamics of Li: Test of a new algorithm, Solid State Commun. 78 (1991) 831.
[23] S. Grimme, S. Ehrlich, L. Goerigk, Effect of the damping function in dispersion corrected density functional theory, Journal of Computational Chemistry 32 (2011) 1456.
[24] V. I. Anisimov, J. Zaanen, O. K. Andersen, Band theory and Mott insulators: Hubbard U instead of Stoner I, Phys. Rev. B 44 (1991) 943–954.
[25] M. Hybertsen, S. Louie, Ab initio static dielectric matrices from the density-functional approach: Formulation and application to semiconductors and insulators, Phys. Rev. B 35 (1987) 5585.
[26] M. Gajdoŝ, K. Hummer, G. Kresse, J. Furthmüller, F. Bechstedt, Linear optical properties in the projector-augmented wave methodology, Phys. Rev. B 73 (2006) 045112.
[27] F. Wooten, Optical Properties of Solids, Academic Press, New York, 1972.
[28] S. Saha, T. P. Sinha, A. Mookerjee, Electronic structure, chemical bonding, and optical properties of paraelectric $BaTiO_3$, Phys. Rev. B 62 (2000) 8828.